ACS Catalysis

pubs.acs.org/acscatalysis Research Article

Rational Engineering of a Membrane-Anchored Promiscuous Cytochrome P450 for the Efficient Biosynthesis of Valuable Ganoderic Acids

Yuhuan Luo,[†] Zeqian Du,[†] Chenjian Jiang,[†] Ziqian Yu, Jian-Jiang Zhong,* Ting Shi,* and Han Xiao*

Cite This: *ACS Catal.* 2023, 13, 15673−15681 Read Online

ACCESS | Metrics & More | Article Recommendations | Supporting Information

ABSTRACT: Lanostane-type triterpenoid ganoderic acids (GAs) possess interesting bioactivities, but their efficient biosynthesis remains challenging. CYP512W2, a promiscuous membrane-anchored cytochrome P450, was recently found to oxidize C7 (or C11) and C15 to form two important GAs, ganoderic acid Y (GA-Y) and ganodermic acid Jb (GA-Jb), but their catalytic routes were unclear. Herein, we report that this CYP exhibits a preference for C7 oxidation, followed by subsequent hydroxylation at C15 after C7 dehydration. Combining computation-aided design with experimental verification, we identified key residues I108, M114, M213, L294, and Y482 critical for CYP512W2 catalytic activity. Engineering these residues significantly increased the production titers of GA-Jb and/or GA-Y. Molecular dynamics analysis uncovered that the proportions of favorable C7- and C15-conformations were enhanced in I108A, and the active pocket and substrate entrance were enlarged in Y482F. Besides, the slightly improved C7-conformation and the reduced C15-conformation in M213R may be attributed to the regulation of substrate conformation mediated by electrostatic attraction. The successful identification of these residues in CYP512W2 provides insights into the design of microbial cell factories for efficient GAs biosynthesis.

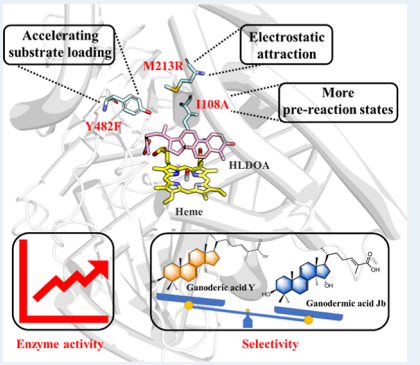

KEYWORDS: *cytochrome P450 (CYP), membrane-anchored, type II ganoderic acids (TIIGAs), molecular dynamics (MD), rational engineering*

1. INTRODUCTION

With conjugated double bonds on the tetracyclic rings, type II ganoderic acids (TIIGAs) are a group of lanostane-type triterpenoids derived from the traditional Chinese medicinal mushroom *Ganoderma lucidum*.[1] As the main medicinal active ingredients, TIIGAs exhibit significant bioactivities, including anticancer,[2] antimetastasis,[3] and hypertensive.[4] Thus, their efficient biosynthesis is of particular importance for revealing the material bases of traditional Chinese medicine as well as accelerating new drug development. However, this is an extremely challenging task due to the complex regulation during TIIGAs biosynthesis,[5] the immature genetic manipulation of medicinal mushrooms,[6] and many unclear cytochrome P450s (CYPs) in the biosynthetic pathway.[7]

To address the above-mentioned scientific questions, as a starting step, we developed a synthetic biology platform to systematically screen Ganoderma-derived 158 CYPs in baker's yeast. A promiscuous CYP512W2, capable of converting type I GA 3-hydroxy-lanosta-8,24-dien-26-oic acid (HLDOA, with one double bond on the tetracyclic rings) into TIIGAs, ganodermic acid Jb (GA-Jb) and ganoderic acid Y (GA-Y), was accordingly identified.[1] In addition to self-possession of biological activities, both GA-Jb and GA-Y are also considered precursors of multiple TIIGAs with more sophisticated modifications and significant bioactivities.

The discovery of CYP512W2 is inspiring since the biosynthesis of GA-Jb and GA-Y can be achieved simultaneously in reactions catalyzed by this single CYP. It is proposed that CYP512W2 first oxidizes either C7 or C11 of HLDOA to form an unstable intermediate and further oxidizes its C15 to form another intermediate, which has been oxidized twice by CYP512W2. The unstable intermediates can be spontaneously transformed into GA-Y and GA-Jb. Meanwhile, CYP512W2 can oxidize C15 of GA-Y to form GA-Jb (Figure 1). We speculated that more than two routes might exist for the transformation of HLDOA into GA-Y and GA-Jb, respectively.[1] But, it is hard to experimentally define which route is most suitable for CYP512W2 due to the instability of the involved intermediates. Herein, we explore its catalytic mechanism and conduct rational protein engineering to increase the catalytic activity and substrate specificity of

Received: September 19, 2023
Revised: November 9, 2023
Accepted: November 9, 2023
Published: November 21, 2023

Downloaded via SHANGHAI JIAO TONG UNIV on November 22, 2023 at 00:35:56 (UTC).
See https://pubs.acs.org/sharingguidelines for options on how to legitimately share published articles.

ACS Publications © 2023 American Chemical Society

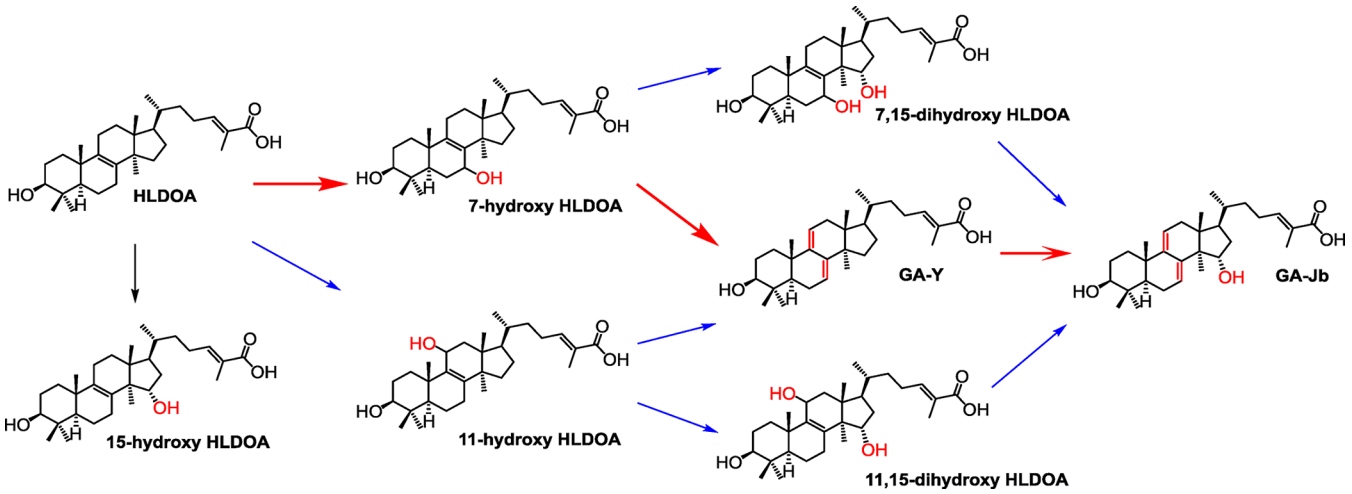

Figure 1. Proposed reaction schemes of the CYP512W2-catalyzed oxidations on HLDOA at C7, C11, and C15. The biosynthetic route from HLDOA to GA-Y and GA-Jb, as elucidated in this work, was highlighted by red arrows.

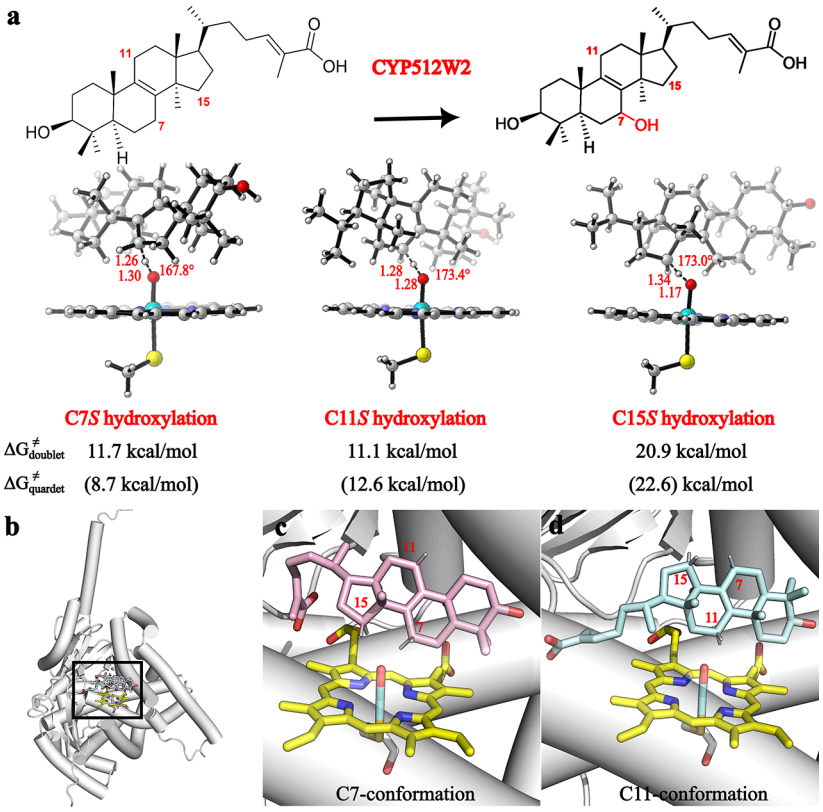

Figure 2. CYP512W2-catalyzed oxidations on HLDOA at C7, C11, and C15. (a) Transition state structures and energy barriers for the hydroxylation of C7*S*, C11*S*, and C15*S*; (b) overview of CYP512W2 with HLDOA at C7- and C11-conformation, respectively; (c) amplified structure of C7-conformation; (d) amplified structure of C11-conformation.

CYP512W2 for the efficient biosynthesis of GA-Jb and/or GA-Y.

In contrast to many reports on the protein engineering of soluble CYPs,[8] there is a lack of work on membrane-anchored P450s. Quantitative analysis of active CYPs in the membrane is quite challenging,[9] not to mention obtaining their crystal structures. Without the guidance of precise structure, engineering targets for increasing catalytic activity and substrate specificity were confined mostly to amino acids in the substrate recognition sites.[10,11]

2. RESULTS AND DISCUSSION

2.1. Mechanistic Insights into CYP512W2-Mediated HLDOA Conversion. In this study, we first predicted the protein structure of CYP512W2 using AlphaFold2 (Figure S1). Based on the comparison of the CYP512W2 sequence with highly similar crystal structures of CYPs in the PDB database, the position of the heme in CYP512W2 was determined. The structure of CYP512W2 exhibited a hydrophobic pocket composed of positively charged residues and interconnected with the substrate access channel (Figure S2). Subsequently,

https://doi.org/10.1021/acscatal.3c04440
ACS Catal. 2023, 13, 15673−15681

HLDOA was docked into the active pocket of CYP512W2. According to the docking results, we confirmed two major conformations, C7- and C11-conformations, which were consistent with the aforementioned proposal. The C7 position was appropriately oriented toward active oxygen (O-heme) of reactive Fe(IV)-oxo radical cation (Cpd I) in C7-conformation, as did C11-conformation (Figure 2). To investigate the CYP512W2-catalyzed oxidations on HLDOA, we constructed a simplified model containing HLDOA and Cpd I with density functional theory (DFT). Hydroxylation at the C7, C11, and C15 positions of HLDOA was studied as the first step of CYP512W2-catalyzed oxidation. Obviously, the hydroxylation at C7 (11.7 kcal/mol) and C11 (11.1 kcal/mol) was more energetically favorable than that at C15 (20.9 kcal/mol), regardless of the enzymatic environment. It is worth noting that the results are still reliable when stereoselectivity (*R* and *S*) and spin state (2 and 4) are taken into account (Figures 2, and S3).

To compare the stability and reaction activity of C7- and C11-conformations in the active pocket of CYP512W2, we performed three independent 100 ns molecular dynamics (MD) simulations starting from the docking results of the C7- and C11-conformations. The key features of the transition state (TS) geometry obtained from the above DFT calculations were used as criteria to assess the hydroxylation possibility of the C7, C11, and C15 positions in the snapshots along the trajectories. They have an O−H distance less than 3.0 Å, the Fe−O−H angle ranging from 100 to 140°, and the C7/C15−H−O angle ranging from 140 to 180°. Conformations falling into these categories were designated as prereactive states (PRS), suggesting they were favorable for hydroxylation. In the MD simulations, the PRS percentage of C7-conformation including both 7*R* and 7*S* (hydroxylation of the pre-*R*/pre-*S* hydrogen at the C7 position of HLDOA) was found to be 13.1%, while it was 0.2% for 15*R* and 6.0% for 15*S*, totaling 6.2% for C15-conformations, which was consistent with the experiment that the major product was 15*S*-GA-Jb. Almost no PRS was observed for C11-conformation. Interestingly, we found that the HLDOA spontaneously underwent flipping from C11-conformation to C7-conformation, generating more favorable PRSs for C7 hydroxylation (Figure S4). Therefore, based on these findings, we concluded that the C7-conformation is more stable and feasible for oxidation than the others in the binding pocket of CYP512W2.

After C7 oxidation was completed, CYP512W2 was able to further convert C7-hydroxylated HLDOA to form GA-Jb via two possible reaction routes. One is C15-hydroxylation took place first, followed by C7-dehydration mediated by a hydrated proton (the direct C15-hydroxylation way), while the second is C7-dehydration, similarly mediated by a hydrated proton, which took place first, followed by C15-hydroxylation (the indirect C15-hydroxylation way). Since the energy barrier for C7-dehydration was calculated to be no more than 10.6 kcal/mol, the reaction route was determined by the energy barrier of hydroxylation, which was calculated to be 17.9 kcal/mol in the direct C15-hydroxylation way and 13.1 kcal/mol in the indirect C15-hydroxylation way. Therefore, we proposed that after the CYP512W2-catalyzed hydroxylation at the C7 position, dehydration took place spontaneously to form GA-Y, and then the hydroxylation at C15 resulted in the generation of GA-Jb (Figures S5 and S6).

2.2. Identification of Key Regulatory Amino Acid Residues of CYP512W2 for Catalytic Activity and Substrate Selectivity.

To better understand the substrate selectivity and further improve the CYP512W2 activity, we tried to select some critical amino acids based on the analysis of MD-simulated protein structures. We initially identified 11 key residues (F104, I108, V112, M114, L123, L294, V295, F297, A298, I361, and S362) based on their significant binding energy with the substrate, each surpassing 0.8 kcal/mol, as determined by MMPBSA binding free energy decomposition. F104, V295, F297, and A298 exhibited high sequence conservation in CYP families, indicating their potential importance for protein structure and function. Thus, we excluded these residues. Given the fact that L123 was located more than 6 Å away from the substrate HLDOA (Figure 3). With such a distance, L123 is unlikely to closely interact with the substrate. Therefore, we excluded this residue. As a result, six variable residues (I108, V112, M114, L294, I361, and S362) that displayed noteworthy binding energy within 6 Å of the substrate were accordingly selected. With the minor side chain and the little impact on α-helical structure, alanine was chosen as the substitution for residues located in α-helical regions (I108A, M114A, and L294A) since such substitution was also frequently used in computational and wet experiments as alanine scanning to verify the performance of specific residues. Without the limitation of the α-helix, residues situated in loop regions were mutated to minimum glycine (I361G and S362G). The residue V112 was centrally located above the substrate. To explore the effect of extending the valine side chain, we introduced the unique mutation V112L (Figure S7a). Here, M210, M213, I364, and Y482, located at the substrate entrance channel, were proposed to play an essential role in the influence of enzymatic activity and substrate selectivity. Our previous study discovered another CYP512A2, which mainly converted HLDOA into GA-Y but had less catalytic activity as compared with CYP512W2.[1] Guided by the entrance channel of CYP512A2, which was highly similar to CYP512W2, M213R, and Y482F were accordingly suggested. Moreover, considering that enlarging the size of the channel entrance usually helps accelerate the rates of substrate entering the catalytic pocket, M210A and I364A were proposed. Taken together, residues M210A, M213R, I364A, and Y482F around the substrate entrance and residues I108A, V112L, M114A, L294A, S362G, and I361G near the active site were picked out for further experimental validation on increasing the catalytic activity and selectivity of CYP512W2 (Figure S7).

Our preliminary test indicated that extracellular HLDOA and GA-Y hardly obtained access to the endoplasmic reticulum-anchored CYPs, making the whole-cell biocatalyst-based assay problematic. To evaluate whether these residues play roles in determining substrate specificity and enzyme catalytic activity, we adopted an in vivo assay. Specifically, CYP512W2 and the mutant expression plasmids, along with the void plasmid pRS426-HXT7p-FBA1t-G418r,[12] were individually introduced into the HLDOA-producing yeast SC62[1] to generate strains SC62-CK, SC62-WT, SC62-I108A, SC62-V112L, SC62-M114A, SC62-M210A, SC62-M213R, SC62-L294A, SC62-I361G, SC62-S362G, SC62-I364A, and SC62-Y482F (Tables S1 and S2). Extracts of 120 h of fermentation from falcon tubes were collected for initial screening. Compared with WT, the production of GA-Jb was increased in I108A and Y482F, while mutations of M114A, M213R, L294A, I361G, and I364A increased the production of GA-Y. Notably, significant increased catalytic activity on

https://doi.org/10.1021/acscatal.3c04440
ACS Catal. 2023, 13, 15673−15681

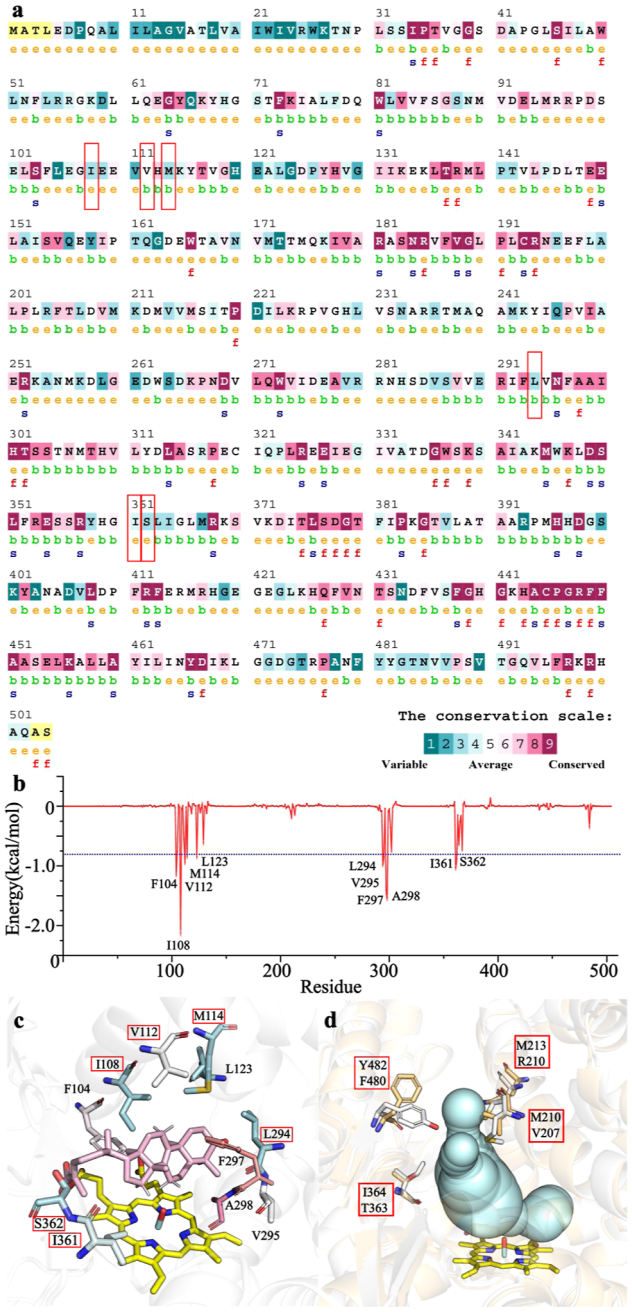

Figure 3. Selected residues for experimental validation by computational analysis. (a) Conservation of the CYP512W2 sequence (analyzed by the ConSurf Web server); (b) key residues contributed more than 0.8 kcal/mol for HLDOA binding; (c) residues contributed more than 0.8 kcal/mol were shown as sticks and colored based on their level of conservation. Selected residues were marked by red rectangles. (d) Residues located at the entrance channel. CYP512W2 and CYP512A2 were colored white and wheat, respectively.

HLDOA was also observed in I108A and Y482F, but a dramatically reduced activity was detected in V112L (Figure S8).

Subsequently, we investigated the fermentation behavior of mutant strains SC62-I108A, SC62-Y482F, SC62-M114A, SC62-M213R, and SC62-L294A in shake flasks. All of the mutants showed different degrees of increased cell growth after 48 h compared with the control strain SC62-WT (Figure 4a). After 120 h, the strains SC62-I108A and SC62-Y482F were able to produce 107.0 and 85.3 mg/L GA-Jb, 2.2- and 1.8-fold higher than that of the control strain (48.8 mg/L), respectively (Figure 4c and Table 1). In contrast, only 8.3 and 7.2 mg/L HLDOA were detected in strains SC62-I108A and SC62-Y482F, 32 and 41% lower than that of the control strain (12.2 mg/L) (Figure 4b), respectively. At the same time, the production of GA-Y by strains SC62-M213R, SC62-L294A, and SC62-M114A reached 46.6, 37.6, and 36.5 mg/L, which was 2.3-, 1.9-, and 1.6-fold higher than that of the control (20.0 mg/L), respectively (Figure 4d).

According to our calculation, the production of GA-Y reflected the selectivity for C7-oxidation, while the production of GA-Jb reflected the selectivity for C7-oxidation and C15-hydroxylation. SC62-I108A and SC62-Y482F indeed exhibited higher GA-Jb production; SC62-L294A, SC62-M114A, and SC62-M213R produced more GA-Y than SC62-WT at different sampling times. For the best mutant, SC62-I108A, after 120 h of fermentation, C15 specificity was improved from 70.9% (by SC62-WT) to 80.7% (Table 1). For SC62-L294A, after 120 h of fermentation, GA-Jb production was comparable with that of SC62-WT (49.5 mg/L vs 48.8 mg/L). However, it should be noted that the production of GA-Y in SC62-L294A was significantly higher than that of SC62-WT (37.6 mg/L vs 20.0 mg/L). In other words, the increased production of GA-Y in SC62-L294A was not at the expense of decreased production of GA-Jb (Figure 4 and Table 1). Thus, we attributed such an evolved phenotype to the higher selectivity at C7-oxidation. For SC-M213R and SC-M114A, their increased productions of GA-Y were accompanied by the reduced production of GA-Jb, demonstrating a reduced C15-hydroxylation and an increased C7-oxidation (Table 1). It should be noted that over 91% of the produced HLDOA was converted by strains SC62-I108A and SC62-Y482F after 48 h fermentation, significantly higher than that from SC62-WT (82.7%). For the rest of the mutants, HLDOA conversion was slightly lower than that of the control strain but at least matched 84% (Table 1).

To determine whether a combination of these beneficial mutations could further contribute to the catalytic activity or substrate selectivity of CYP512W2, we constructed double mutants SC62-I108A-Y482F, SC62-M114A-M213R, SC62-M114A-L294A, SC62-M213R-L294A, and triple mutant SC62-M114A-M213R-L294A (Tables S1 and S2). During the whole fermentation process in shake flasks, the cell growth of these engineered strains was comparable to that of SC62-WT (Figure 5a). For double mutants SC62-M114A-L294A, SC62-M114A-M213R, and SC62-M213R-L294A, they produced 38.2, 41.0, and 48.1 mg/L GA-Y after 120 h fermentation, respectively, with significantly higher production selectivity of GA-Y (83.4, 84.9, and 84.2%, respectively) than that from their corresponding single mutants (Figures 4d and 5d and Tables 1 and S3). Among them, the production titers of GA-Y in strains SC62-M114A-L294A and SC62-M213R-L294A were also higher than those from their corresponding single mutants (Figures 4d, 5d, Tables 1 and S3). Surprisingly, both GA-Y and GA-Jb production in triple mutant SC62-M114A-M213R-L294A were dramatically reduced (6.7 mg/L GA-Y and 2.8 mg/L GA-Jb after 120 h fermentation), accompanied by 79.7 mg/L HLDOA accumulated after 120 h (Figure 5b–d).

2.3. Deciphering the Structural Characteristics of CYP512W2 Mutants. In order to reveal the molecular

https://doi.org/10.1021/acscatal.3c04440
ACS Catal. 2023, 13, 15673−15681

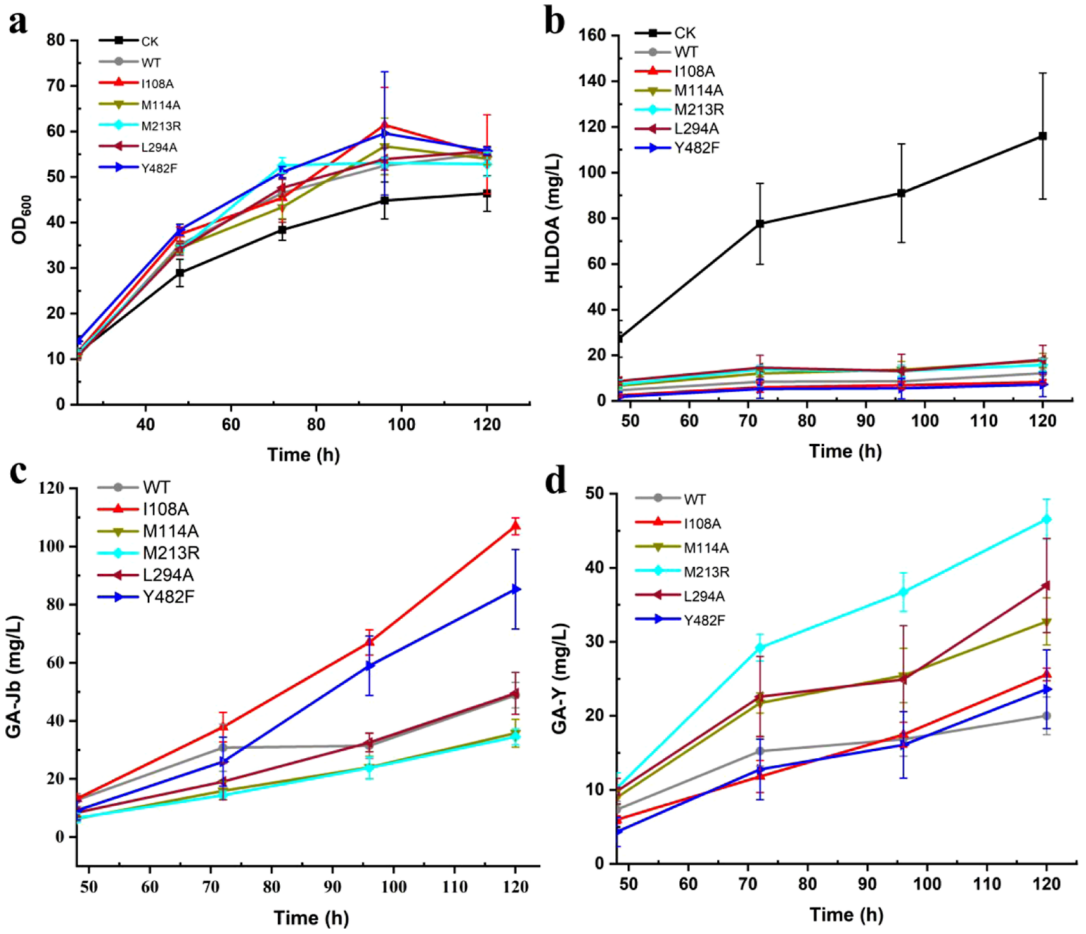

Figure 4. Time profile of (a) cell growth, (b) accumulation of HLDOA, and production of (c) GA-Jb and (d) GA-Y in shake flask fermentation of strains SC62-CK, SC62-WT, SC62-I108A, SC62-M114A, SC62-M213R, SC62-L294A, and SC62-Y482F. The error bars represent the standard deviation of five biological replicates.

Table 1. Selectivity, Conversion, and the Production Change of Selective Mutants to Generate GA-Jb and GA-Y

time (h)	SC62-WT	SC62-I108A	SC62-M114A	SC62-M213R	SC62-L294A	SC62-Y482F
			selectivity % (Jb/Y)[a]			
48	63.5%/36.5%	68.9%**/31.1%**	41.2%**/58.8%**	39.2%**/60.8%**	46.0%**/54.0%**	67.8%*/32.2%*
72	66.9%/33.1%	76.2%**/23.8%**	42.3%**/57.7%**	33.0%**/67.0%**	45.8%**/54.2%**	67.0%/33.0%
96	65.1%/34.9%	79.3%**/20.7%**	48.5%**/51.5%**	39.3%**/60.7%**	56.6%/43.4%	78.6%**/21.4%**
120	70.9%/29.1%	80.7%**/19.3%**	52.2%**/47.8%**	42.6%**/57.4%**	56.8%**/43.2%**	78.3%**/21.7%**
			conversion %[b]			
48	82.7%	91.0%*	75.2%	73.4%	68.2%	93.3%**
72	89.1%	92.3%	84.4%	82.2%*	81.2%	93.2%*
96	90.6%	92.5%	85.0%	85.6%	85.5%	93.9%
120	89.5%	92.8%	84.8%	86.4%	84.4%	93.8%
			production of Jb/Y as compared with SC62-WT %[c]			
48	100%	103.5%/81.6%*	49.2%**/122.7%	51.7%**/139.9%	65.7%**/134.1%	71.5%**/59.2%*
72	100%	123.1%/77.5%*	51.8%**/142.7%*	46.8%**/191.6%**	62.1%/148.2%	84.4%/83.7%
96	100%	212.9%**/103.6%	76.2%*/151.1%*	75.6%**/217.9%**	103.3%/147.8%	187.3%**/95.5%
120	100%	219.1%**/127.9%*	73.2%*/163.7%**	70.8%**/232.7%**	101.4%/188.0%*	174.8%**/118.0%

[a]Selectivity refers to the ratio of GA-Jb or GA-Y titers in the total titers of GA-Jb and GA-Y. [b]Conversion refers to the ratio of consumed HLDOA (the difference of the HLDOA titer by strain SC62-CK and the corresponding mutants) to the total titer of HLDOA (HLDOA produced by strain SC62-CK). *$p < 0.05$; **$p < 0.01$. [c]Production of Jb/Y as compared with SC62-WT% refers to the ratio of the GA-Jb/Y production titer of the mutant to that of the WT.

mechanism for its improvement in activity and selectivity for producing GA-Jb in SC62-I108A, an additional three times 100 ns of MD simulations were performed. We modified the WT model by replacing I108 with A108 at the C7-conformation of WT containing HLDOA and Cpd I. By comparing the trajectories of I108A with WT, we found I108A showed more PRSs than that in WT. The percentage of PRSs in WT was 5.4% for C7*R* (hydroxylation of the pre-*R* hydrogen at the C7

https://doi.org/10.1021/acscatal.3c04440
ACS Catal. 2023, 13, 15673−15681

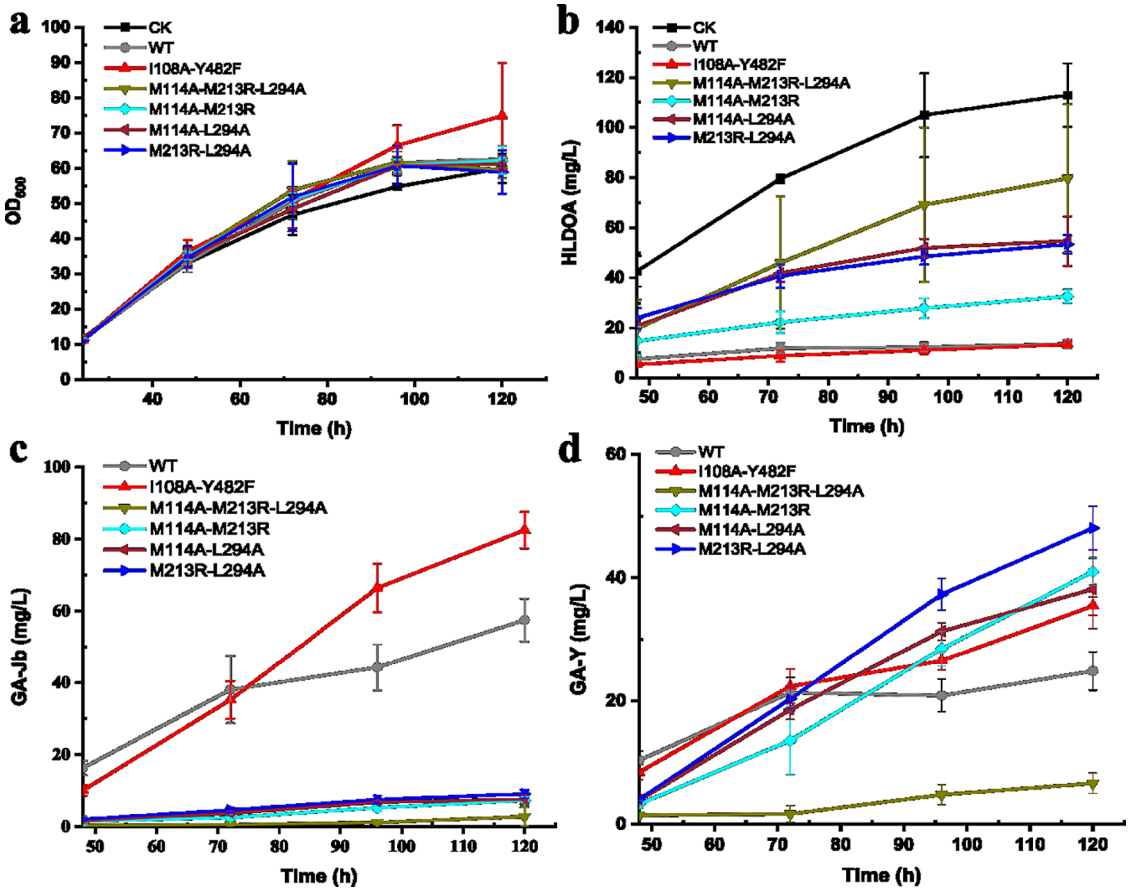

Figure 5. Time profile of (a) cell growth, (b) accumulation of HLDOA, production of (c) GA-Jb and (d) GA-Y in shake flask fermentation of strains SC62-CK, SC62-WT, SC62-I108A-Y482F, SC62-M114A-M213R, SC62-M114A-L294A, SC62-M213R-L294A, and SC62-M114A-M213R-L294A. The error bars represent the standard deviation of five biological replicates.

position of HLDOA), 7.7% for C7*S* (pre-*S* hydrogen), and 6.0% for C15*S*, respectively, while that was 21.6% for C7*R*, 7.3% for C7*S*, and 33.1% for C15*S* in the I108A model (Figures 6 and S4a). These results indicated that I108A provided more favorable PRSs for oxidation at both C7 and C15 positions, which might finally result in the improvement of CYP512W2 activity and selectivity.

On the other hand, to understand the function of Y482F, which is located in the substrate entrance channel of CYP512W2, we conducted steered molecular dynamic (SMD) simulations in the WT and Y482F models to compare how hard it is for HLDOA to get in and out of the pocket. The results demonstrated that the potential mean force for pulling HLDOA out of the catalytic pocket was reduced by a third in the Y482F model, indicating that the Y482F mutation is favorable for the loading of HLDOA and further improving the catalytic activity of CYP512W2 (Figure S9).

Subsequently, we conducted molecular simulations to investigate models M213R and M114A-M213R individually, employing the same methodology as that outlined earlier for the I108A model. These mutations represent the single and double mutants with the highest selectivity for Gb-Y, respectively. For M213R, we observed a stable electrostatic attraction between the guanidyl group of R213 and the terminal carboxyl group of HLDOA. This interaction stabilized more favorable C7-conformations over C15-conformations. Specifically, the percentage of PRSs in M213R was 15.6% for C7*R* (higher than WT of 5.4%) and 2.4% for C15*S* (lower than WT of 6.0%). Consequently, this led to increased production of the GA-Y product (Figure S10). In the case of M114A-M213R, the percentages of PRSs were 6.8% for C7*R* and 0.2% for C15*S*. These results unveiled that, apart from the stable electrostatic interaction between R213 and the carboxyl group of HLDOA, the substitution of A114 provided more spatial freedom than M114. This allowed HLDOA to move slightly further away from the active oxygen (O-heme) of the reactive Cpd I, reducing the opportunities for C15 hydroxylation and thereby enhancing C7 specificity (Figure S11, where C7 is closer to the active oxygen of Cpd I than C15). Consequently, M114A-M213R was found to significantly improve GA-Y production, albeit at the cost of reduced conversion efficiency. We performed molecular dynamics (MD) simulations to investigate the reasons for the reduced activity of the triple mutant M114A-M213R-L294A. It revealed that the pre-reaction states were only 1.7 and 1.8% for C7- and C15-hydroxylation in the triple mutant (Figure S12a), which still remained at 13.1 and 6.2% in the WT (Figure S4a), respectively. As expected, the carboxyl group of the substrate was fixed by R213 through electrostatic attraction. However, the mutations of M114A and L294A created a larger space in the active site, which was inappropriate to lock the conformation of the substrate. As a result, the substrate was observed to change from a standing position to a lying-down orientation, far away from active oxygen (O-heme) (Figure S12b,c). Collectively, the triple mutant exhibited the instability

https://doi.org/10.1021/acscatal.3c04440
ACS Catal. 2023, 13, 15673−15681

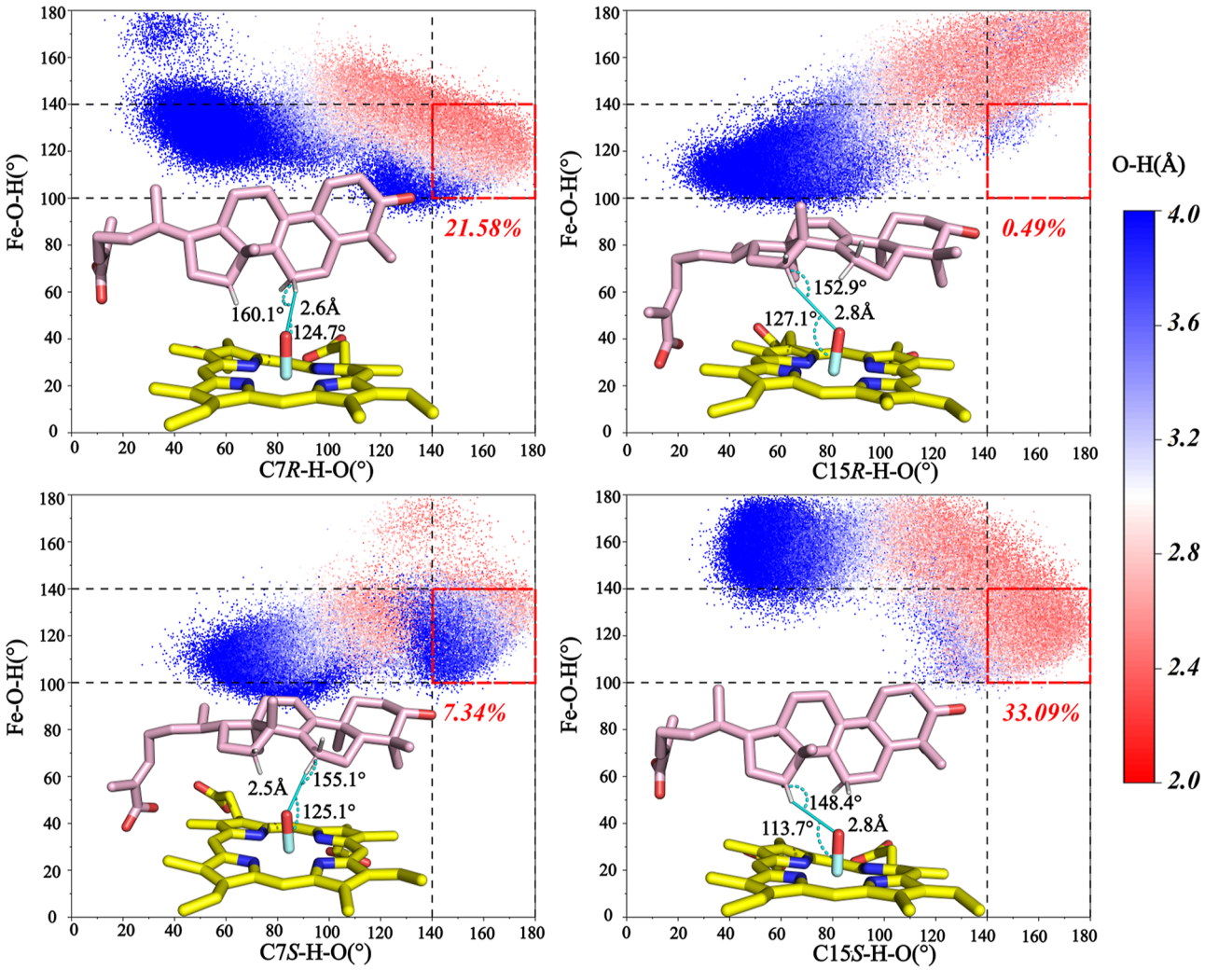

Figure 6. Percentage of PRSs hydroxylated at C7 and C15 of HLDOA in I108A mutant simulations.

of substrate shifting away from the active O-heme and low catalytic activity in producing GA-Y and GA-Jb.

The MD simulation combined with the QM calculation revealed that CYP512W2 might prefer to perform C7- and C15-oxidation on the tetracyclic ring of triterpenoid. Identification of the key regulatory residues indicated that CYP512W2 employed different mechanisms to control catalytic activity and substrate selectivity. For C7 oxidation, a fungal-derived CYP5150AP3 was reported to catalyze C7β hydroxylation of testosterone and 11-deoxycortisol, with a similar skeleton as triterpenoid.[13] To the best of our knowledge, such regulatory residues have not been identified in membrane-anchored CYPs. For bacterial-derived soluble CYPs, CYP102A1 was the most studied for C7 hydroxylation of steroids. A328G and I263G were responsible for C7α hydroxylation, while F81I and M177T were related to C7β hydroxylation in CYP102A1.[14,15] For the mutant with selective oxidation on C7 identified in this work, L294A was conservative to I263G in CYP102A1, suggesting that the mechanism for controlling C7 oxidation may be general applicable in fungal-derived membrane-anchored CYPs. For C15 oxidation, $P450_{pra}$ from *Penicillium raistrickii* was identified as the C15α hydroxylase of the steroid, but its regulatory residues remained obscure.[16] Interestingly, the F483I mutant of a human-derived CYP2D6, one of the few membrane-anchored CYPs with crystal structure, showed enhanced activity on C15 hydroxylation of testosterone.[17] Along with this observation, the Y482F identified in this study showed conservation with F483I in CYP2D6. The conservation of this key residue was identified in different CYP families, indicating that membrane-anchored CYPs may share a common mechanism to control the C15 oxidation of the tetracyclic ring.

3. CONCLUSIONS

In summary, we successfully identified key residues (I108, M114, M213, L294, and Y482) that are critical for catalytic activity. Engineering these residues multiplied the production titers of two valuable GAs (GA-Y and GA-Jb). These findings provide insights for designing a microbial cell factory for GAs production and open the door for further deconvolution of the complex biosynthetic pathway of other important TIIGAs.

■ ASSOCIATED CONTENT

Supporting Information

The Supporting Information is available free of charge at https://pubs.acs.org/doi/10.1021/acscatal.3c04440.

Experimental procedures; general materials and methods; prediction of the structure of CYP512W2 and

https://doi.org/10.1021/acscatal.3c04440
ACS Catal. 2023, 13, 15673−15681

CYP512A2; MD simulations; adaptive steered MD simulations; QM calculations; cloning and expression of CYP512W2 and its associated mutants; fermentation in a falcon tube; fermentation in a shake flask; construction of plasmids; strains used in this study; selectivity, conversion, and the production change of double and triple mutants to generate GA-Jb and GA-Y; predicted CYP512W2 structure and the plDDT scores from AlphaFold2; structure of CYP512W2; transition state structures obtained from QM calculations; proportion and structure analysis of PRSs for C7-conformation and C11-conformation; proposed reaction route for generation of GA-Jb in the direct C15-hydroxylation way; proposed reaction route for generation of GA-Jb in the indirect C15-hydroxylation way; selected residues for experimental validation; initial screening of CYP512W2 mutants on the production of GA-Jb and GA-Y; structural snapshots of HLDOA loading; proportion and structure analysis of PRSs for the M213R model; proportion and structure analysis of PRSs for the M114A-M213R model; proportion and structure analysis of PRSs for the mutant M114A-M213R-L294A; and supplementary references (PDF)

AUTHOR INFORMATION

Corresponding Authors

Jian-Jiang Zhong − *State Key Laboratory of Microbial Metabolism, Joint International Research Laboratory of Metabolic & Developmental Sciences, School of Life Sciences and Biotechnology, Shanghai Jiao Tong University, Shanghai 200240, China;* orcid.org/0000-0002-2265-9338; Email: jjzhong@sjtu.edu.cn

Ting Shi − *State Key Laboratory of Microbial Metabolism, Joint International Research Laboratory of Metabolic & Developmental Sciences, School of Life Sciences and Biotechnology, Shanghai Jiao Tong University, Shanghai 200240, China;* orcid.org/0000-0003-3921-4412; Email: tshi@sjtu.edu.cn

Han Xiao − *State Key Laboratory of Microbial Metabolism, Joint International Research Laboratory of Metabolic & Developmental Sciences, School of Life Sciences and Biotechnology, Shanghai Jiao Tong University, Shanghai 200240, China;* orcid.org/0000-0003-2895-1847; Email: smallhan@sjtu.edu.cn

Authors

Yuhuan Luo − *State Key Laboratory of Microbial Metabolism, Joint International Research Laboratory of Metabolic & Developmental Sciences, School of Life Sciences and Biotechnology, Shanghai Jiao Tong University, Shanghai 200240, China*

Zeqian Du − *State Key Laboratory of Microbial Metabolism, Joint International Research Laboratory of Metabolic & Developmental Sciences, School of Life Sciences and Biotechnology, Shanghai Jiao Tong University, Shanghai 200240, China*

Chenjian Jiang − *State Key Laboratory of Microbial Metabolism, Joint International Research Laboratory of Metabolic & Developmental Sciences, School of Life Sciences and Biotechnology, Shanghai Jiao Tong University, Shanghai 200240, China*

Ziqian Yu − *State Key Laboratory of Microbial Metabolism, Joint International Research Laboratory of Metabolic & Developmental Sciences, School of Life Sciences and Biotechnology, Shanghai Jiao Tong University, Shanghai 200240, China*

Complete contact information is available at: https://pubs.acs.org/10.1021/acscatal.3c04440

Author Contributions

H.X. and T.S. conceived and designed the study. H.X., T.S., and Z.D. wrote the manuscript. Y.L. constructed the CYP expression plasmids and yeast-engineered strains with the partial participation of C.J. and Z.Y. Y.L. and C.J. performed the fermentation assay of yeast strains and analyzed the HPLC data. Z.D. and T.S. performed the QM calculations, MD simulations, and other computational analyses. H.X., T.S., and J.J.Z. finalized the manuscript. All authors concur with the submission, have seen a draft copy of the manuscript, and agree with its publication.

Author Contributions

†Y.L., Z.D., and C.J. contributed equally to this work.

Notes

The authors declare no competing financial interest.

ACKNOWLEDGMENTS

This work was supported in part by the National Key R&D Program of China (2018YFA0900600 to H.X. and 2021YFC2100601 to T.S.) and the NSFC (31971344 to H.X. and 32270038 to T.S.). H.X. thanks the DaSilva Award (The Society for Biotechnology, Japan) for financial support. The computations were performed on the π 2.0 cluster supported by the Center for High Performance Computing at Shanghai Jiao Tong University.

REFERENCES

(1) Yuan, W.; Jiang, C.; Wang, Q.; Fang, Y.; Wang, J.; Wang, M.; Xiao, H. Biosynthesis of mushroom-derived type II ganoderic acids by engineered yeast. *Nat. Commun.* **2022**, *13* (1), 7740.

(2) Jiang, Z. J.; Jin, T. T.; Gao, F.; Liu, J. W.; Zhong, J. J.; Zhao, H. Effects of ganoderic acid Me on inhibiting multidrug resistance and inducing apoptosis in multidrug resistant colon cancer cells. *Process Biochem.* **2011**, *46* (6), 1307−1314.

(3) Chen, N. H.; Liu, J. W.; Zhong, J. J. Ganoderic acid T inhibits tumor invasion in vitro and in vivo through inhibition of MMP expression. *Pharmacol. Rep.* **2010**, *62* (1), 150−163.

(4) Wei, J. C.; Wang, A. H.; Wei, Y. L.; Huo, X. K.; Tian, X. G.; Feng, L.; Ma, X. C.; Wang, C.; Huang, S. S.; Jia, J. M. Chemical characteristics of the fungus Ganoderma lucidum and their inhibitory effects on acetylcholinesterase. *J. Asian Nat. Prod. Res.* **2018**, *20* (10), 992−1001.

(5) Hirotani, M.; Furuya, T. Changes of the triterpenoid patterns during formation of the fruit body in Ganoderma lucidum. *Phytochemistry* **1990**, *29* (12), 3767−3771.

(6) Kim, S.; Ha, B. S.; Ro, H. S. Current technologies and related issues for mushroom transformation. *Mycobiology* **2015**, *43* (1), 1−8.

(7) Xiao, H.; Zhang, Y.; Wang, M. Discovery and engineering of cytochrome P450s for terpenoid biosynthesis. *Trends Biotechnol.* **2019**, *37* (6), 618−631.

(8) Li, A. T.; Qu, G.; Sun, Z. T.; Reetz, M. T. Statistical analysis of the benefits of focused saturation mutagenesis in directed evolution based on reduced amino acid alphabets. *ACS Catal.* **2019**, *9* (9), 7769−7778.

(9) Guengerich, F. P.; Martin, M. V.; Sohl, C. D.; Cheng, Q. Measurement of cytochrome P450 and NADPH-cytochrome P450 reductase. *Nat. Protoc.* **2009**, *4* (9), 1245−1251.

(10) Song, F.; Zheng, M.; Wang, J.; Liu, H.; Lin, Z.; Liu, B.; Deng, Z.; Cong, H.; Zhou, Q.; Qu, X. Chemoenzymatic synthesis of C14-functionalized steroids. *Nat. Synth.* **2023**, *2*, 729−739.
(11) Romsuk, J.; Yasumoto, S.; Seki, H.; Fukushima, E. O.; Muranaka, T. Identification of key amino acid residues toward improving the catalytic activity and substrate specificity of plant-derived cytochrome P450 monooxygenases CYP716A subfamily enzyme for triterpenoid production in Saccharomyces cerevisiae. *Front. Bioeng. Biotechnol.* **2022**, *10*, 955650.
(12) Lan, X.; Yuan, W.; Wang, M.; Xiao, H. Efficient biosynthesis of antitumor ganoderic acid HLDOA using a dual tunable system for optimizing the expression of CYP5150L8 and a Ganoderma P450 reductase. *Biotechnol. Bioeng.* **2019**, *116* (12), 3301−3311.
(13) Lu, W.; Feng, J.; Chen, X.; Bao, Y. J.; Wang, Y.; Wu, Q.; Ma, Y.; Zhu, D. Distinct regioselectivity of fungal P450 enzymes for steroidal hydroxylation. *Appl. Environ. Microbiol.* **2019**, *85* (18), No. e01182−01119.
(14) Chen, W. Y.; Fisher, M. J.; Leung, A.; Cao, Y.; Wong, L. L. Oxidative diversification of steroids by nature-inspired scanning glycine mutagenesis of P450BM3 (CYP102A1). *ACS Catal.* **2020**, *10* (15), 8334−8343.
(15) Li, A. T.; Acevedo-Rocha, C. G.; D'Amore, L.; Chen, J. F.; Peng, Y. Q.; Garcia-Borras, M.; Gao, C. H.; Zhu, J. M.; Rickerby, H.; Osuna, S.; Zhou, J. H.; Reetz, M. T. Regio- and stereoselective steroid hydroxylation at C7 by cytochrome P450 monooxygenase mutants. *Angew. Chem., Int. Ed.* **2020**, *59* (30), 12499−12505.
(16) Jia, L.; Dong, J.; Wang, R.; Mao, S.; Lu, F.; Singh, S.; Wang, Z.; Liu, X. Identification and characterization of the steroid 15α-hydroxylase gene from Penicillium raistrickii. *Appl. Microbiol. Biotechnol.* **2017**, *101* (16), 6409−6418.
(17) Smith, G.; Modi, S.; Pillai, I.; Lian, L. Y.; Sutcliffe, M. J.; Pritchard, M. P.; Friedberg, T.; Roberts, G. C.; Wolf, C. R. Determinants of the substrate specificity of human cytochrome P-450 CYP2D6: design and construction of a mutant with testosterone hydroxylase activity. *Biochem. J.* **1998**, *331* (3), 783−792.

NOTE ADDED AFTER ASAP PUBLICATION

This paper was originally published ASAP on November 21, 2023, before all corrections were received. The updated version was reposted on November 21, 2023.

https://doi.org/10.1021/acscatal.3c04440
ACS Catal. 2023, 13, 15673−15681